

# Strain-induced metal-insulator transition in $t_{2g}$ electron system of perovskite titanate $\text{Sm}_{0.5}\text{Ca}_{0.5}\text{TiO}_3$ films

K. Yoshimatsu,<sup>1,\*</sup> H. Okabe,<sup>1,†</sup> T. Oshima,<sup>1</sup> S. Ueda,<sup>2,3</sup> and A. Ohtomo<sup>1,4,†</sup><sup>1</sup>*Department of Applied Chemistry, Tokyo Institute of Technology, 2-12-1 Ookayama, Meguro-ku, Tokyo 152-8552, Japan*<sup>2</sup>*Synchrotron X-ray Station at SPring-8, National Institute for Materials Science (NIMS), Sayo, Hyogo 679-5148, Japan*<sup>3</sup>*Quantum Beam Unit, NIMS, Tsukuba 305-0047, Japan*<sup>4</sup>*Materials Research Center for Element Strategy (MCES), Tokyo Institute of Technology, Yokohama 226-8503, Japan*

(Received 11 November 2015; revised manuscript received 25 April 2016; published 27 May 2016)

We have demonstrated a strain-induced metal-insulator transition for weak Jahn-Teller effects in a  $t_{2g}$  electron system of  $\text{Sm}_{0.5}\text{Ca}_{0.5}\text{TiO}_3$ , which has metallic ground states in the bulk. A clear variation of electronic properties in  $\text{Sm}_{0.5}\text{Ca}_{0.5}\text{TiO}_3$  thin films was investigated as a function of epitaxial strain by changing a substrate and the film thickness. Under strong biaxial tensile strain, metallic behaviors were completely eliminated, as evidenced by the temperature dependence of resistivity. The observed metal-insulator transition was consistent with the behavior of the Ti 3d density of states at the Fermi level seen in valence band hard x-ray photoemission spectra.

DOI: [10.1103/PhysRevB.93.195159](https://doi.org/10.1103/PhysRevB.93.195159)

## I. INTRODUCTION

Advances in thin-film-growth techniques by using pulsed-laser deposition (PLD) have enabled us to create high-quality oxide films [1,2]. Gigantic pressures up to  $\sim 10$  GPa can be induced in heteroepitaxial films grown on prescribed substrates [3,4]. For strongly correlated electron systems, the resulting strain drastically influences their physical properties that are sensitive to spin, charge, orbital, and lattice degrees of freedom [5,6]. Using PLD, Konishi *et al.* investigated a systematic variation of electronic and magnetic properties in perovskite manganites,  $\text{La}_{1-x}\text{Sr}_x\text{MnO}_3$  (LSMO), as a function of epitaxial strain [3]. They created ferromagnetic metal, A-type antiferromagnetic metal, and C-type antiferromagnetic insulator films in LSMO with  $x = 0.5$ , which were grown on  $(\text{LaAlO}_3)_{0.3}\text{-(SrAl}_{0.5}\text{Ta}_{0.5}\text{O}_3)_{0.7}$  (LSAT),  $\text{SrTiO}_3$ , and  $\text{LaAlO}_3$  (100) substrates, respectively. Rate *et al.* reported a strain-induced metal-insulator transition (MIT) in  $\text{La}_{0.7}\text{Ca}_{0.3}\text{CoO}_3$  films grown on piezoelectric  $\text{Pb}(\text{Mg}_{1/3}\text{Nb}_{2/3})_{0.72}\text{Ti}_{0.28}\text{O}_3$  substrates by PLD [7]. For samples exhibiting ferromagnetic insulating states, room-temperature resistivity was found to reversibly change by an order of magnitude upon varying the spontaneous polarization of the substrates. These attractive works focused on the modulation of the electronic and magnetic states in  $e_g$  electron systems [3,4,7–11]. The  $e_g$  orbitals of transition-metal (B) ions are extended toward the  $2p$  orbitals of oxide ions and thus their configurations are sensitive to the distortions of  $\text{BO}_6$  octahedra, providing the possibility for strain-induced modulation of the physical properties. In contrast, strain-induced effects such as MIT are rarely known for  $t_{2g}$  electron systems, e.g., heteroepitaxial films of perovskite titanates and vanadates.

Perovskite titanates  $\text{Ln}^{3+}\text{TiO}_3$  ( $\text{Ln} =$  lanthanide ions) with the  $t_{2g}^1$  configuration at half filling are typical Mott-Hubbard

insulators, among which we focus on  $\text{SmTiO}_3$  (SmTO) having a heavily distorted  $\text{GdFeO}_3$ -type structure (Ti-O-Ti bond angle of  $147^\circ$ ) [12,13]. Substitution of divalent alkaline-earth ions to trivalent lanthanide ones in the  $\text{Ln}^{3+}\text{TiO}_3$  causes hole doping to the  $\text{Ti}^{3+}$  ions, leading to a transition from insulator to metal. Katsufuji *et al.* grew single crystals of  $\text{Sm}_{1-x}\text{Ca}_x\text{TiO}_3$  in the form of a solid solution of  $\text{CaTiO}_3$  (CTO) and SmTO to investigate the effects of A-site substitution [14]. The transition from insulator to metal occurred in a range of  $0.20 \leq \delta \leq 0.24$ , where  $\delta$  is the number of holes at the Ti site given by the sum of  $x$  and  $y$  in  $\text{Sm}_{1-x}\text{Ca}_x\text{TiO}_{3+y/2}$ . The critical  $\delta$  was larger than that of  $\text{La}_{1-x}\text{Sr}_x\text{TiO}_3$  [15] because of the smaller bandwidth of  $\text{Sm}_{1-x}\text{Ca}_x\text{TiO}_3$ . In contrast of filling control by chemical substitution, MIT by application of hydrostatic pressure or epitaxial strain has not yet been observed for  $\text{Ln}^{3+}\text{TiO}_3$ , regardless of sample form and chemical composition. As for the *insulator-to-metal* transition, there is a seminal work by He *et al.*, where insulating  $\text{LaTiO}_3$  films grown by PLD turned to a metallic phase when compressive biaxial strain was applied [16].

In this paper, we have studied the structural and electronic properties of  $\text{Sm}_{0.5}\text{Ca}_{0.5}\text{TiO}_3$  (SCTO) films with the metallic ground state to demonstrate MIT by application of *tensile* biaxial strain. We prepared a series of SCTO films grown on  $\text{NdGaO}_3$  (NGO) (110), LSAT (100), and  $\text{DyScO}_3$  (DSO) (110) substrates. The films on the NGO and LSAT substrates represented metallic conductivity as expected from the bulk properties, owing to relatively small strain. On the other hand, the film coherently grown on the DSO substrate showed insulating behavior. In addition, the strength of the MIT (resistivity at room temperature) systematically decreased with increasing film thickness. Moreover, we have performed hard x-ray photoemission spectroscopy (HXPES) to investigate the electronic structures of two distinct phases. A difference in the Ti 3d derived density of states (DOS) at the Fermi level ( $E_F$ ) was clearly found between the metallic and insulating SCTO films.

## II. EXPERIMENTS

A SCTO ceramic tablet was prepared by a conventional solid-state reaction method. Regent-grade  $\text{CaCO}_3$ ,  $\text{TiO}_2(4N)$ ,

\* Author to whom correspondence should be addressed: k-yoshi@apc.titech.ac.jp

† Present address: Department of Chemical Science and Engineering, Tokyo Institute of Technology, 2-12-1 Ookayama, Meguro-ku, Tokyo 152-8552, Japan.

$\text{Sm}_2\text{O}_3$ , and Ti (3N) powders with a molar ratio of 4:7:2:1 were mixed and pressed into a pellet. It was sintered at 1100 °C for 12 h in vacuum. The powder x-ray diffraction (XRD) measurement using Cu  $K\alpha$  radiation confirmed a perovskite phase with a slight amount of the oxidized pyrochlore phase.

Prior to the film growth, DSO, NGO, and LSAT substrates were annealed in air to obtain a step-and-terrace surface [17–19]. The annealed temperatures and duration times were 1000 °C and 4 h (DSO), 1000 °C and 2 h (NGO), and 1200 °C and 5 h (LSAT). The films were grown by using PLD in an ultrahigh-vacuum chamber equipped with reflection high-energy electron diffraction (RHEED). KrF excimer laser pulses (5 Hz, 1.0 J/cm<sup>2</sup>) were focused on the SCTO ceramic tablet. The growth temperature was set to about 825 °C. An Ar gas (6N purity) was continuously fed into the chamber to keep the chamber pressure at 10<sup>-6</sup> Torr. After the growth, the samples were quenched to room temperature (200 °C/min in average) in Ar atmosphere to prevent oxidation.

The epitaxial structures were characterized using a laboratory XRD apparatus with Cu $K\alpha_1$  radiation. The surface morphology was observed by atomic force microscopy (AFM). The temperature dependence of resistivity was measured by a standard four-probe method using a physical property measurement system (Quantum Design PPMS). HXPES measurements were carried out at the undulator beamline BL15XU [20,21] of SPring-8. All spectra were taken at room temperature using a high-resolution hemispherical electron analyzer (VG Scienta, R4000).  $E_F$  was referred to that of an evaporated Au thin film electronically in contact with the samples. The total energy resolution was set to about 230 meV at an excitation photon energy of 5.95 keV.

### III. RESULTS AND DISCUSSION

Figure 1(a) shows RHEED intensity oscillation during the growth of SCTO films (~50 nm) on DSO substrates. Long-lasting and clear intensity oscillations were seen, indicating a two-dimensional growth mode. The film thickness referred to in the following was determined by assuming that a single unit cell (~0.4 nm) grew during the oscillation period (5.2 s). The RHEED image taken after the growth showed clear streaks with spacing identical to that of the substrate. An atomically flat surface with step-and-terrace structures was found in the AFM image [inset of Fig. 1(a)]. A well-defined surface structure endorses a high-quality crystal and contributes to high-quality HXPES measurements. Figure 1(b) shows the out-of-plane XRD pattern around 220 DSO reflections. A 220 SCTO reflection was detected at 46.33° at the higher angle side of the 220 DSO reflections. No secondary phase (such as pyrochlore) was found in a full-range XRD pattern (not shown) [22]. In addition, clear Laue fringes were seen around the 220 SCTO reflections, reflecting high crystalline quality. A thickness of 46 nm estimated from the spacing of Laue fringes was in good agreement with the design. These results, including a sharp x-ray rocking curve with a full width at half maximum (FWHM) of 0.086° [Fig. 1(c)], are essential to discuss the following results.

The MIT of SCTO films was investigated by the temperature dependence of resistivity as shown in Fig. 2. The resistivity of the film (50 nm) on the DSO (110) substrate was on the

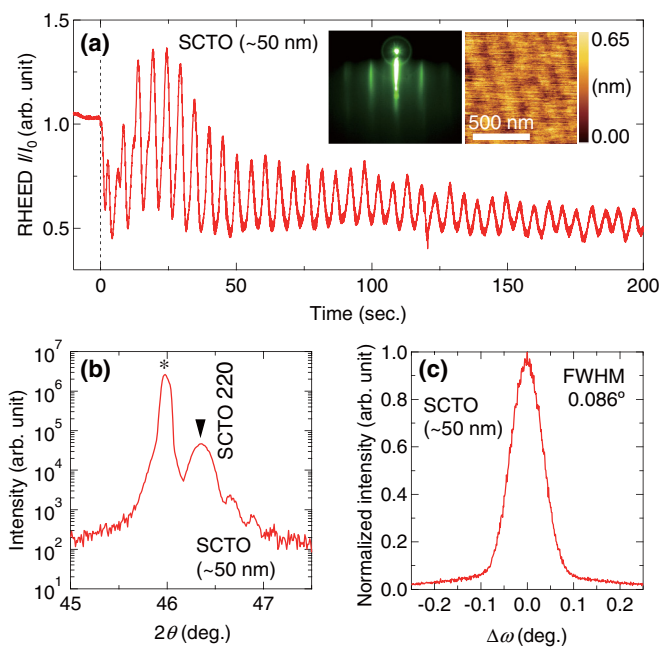


FIG. 1. Characterization of the SCTO films on the DSO substrates. (a) RHEED intensity oscillations for the specular beam spot during the initial growth. The insets show the RHEED and AFM images of the SCTO film. (b) Out-of-plane XRD pattern around 220 DSO reflections (indicated by the asterisk). The 220 SCTO reflection is indicated by the solid triangle. (c) X-ray rocking curves of 220 SCTO reflections.

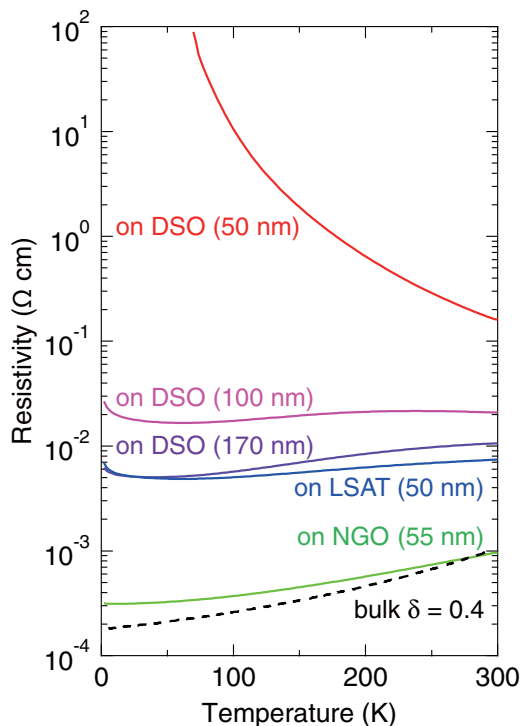


FIG. 2. Temperature dependence of resistivity for the SCTO films. The curves for the films on DSO substrates' thickness dependence, while those with thickness of 50–55 nm on DSO, LSAT, and NGO strain dependence. The dashed curve indicates the bulk single crystal ( $\delta = 0.4$ ) [14].

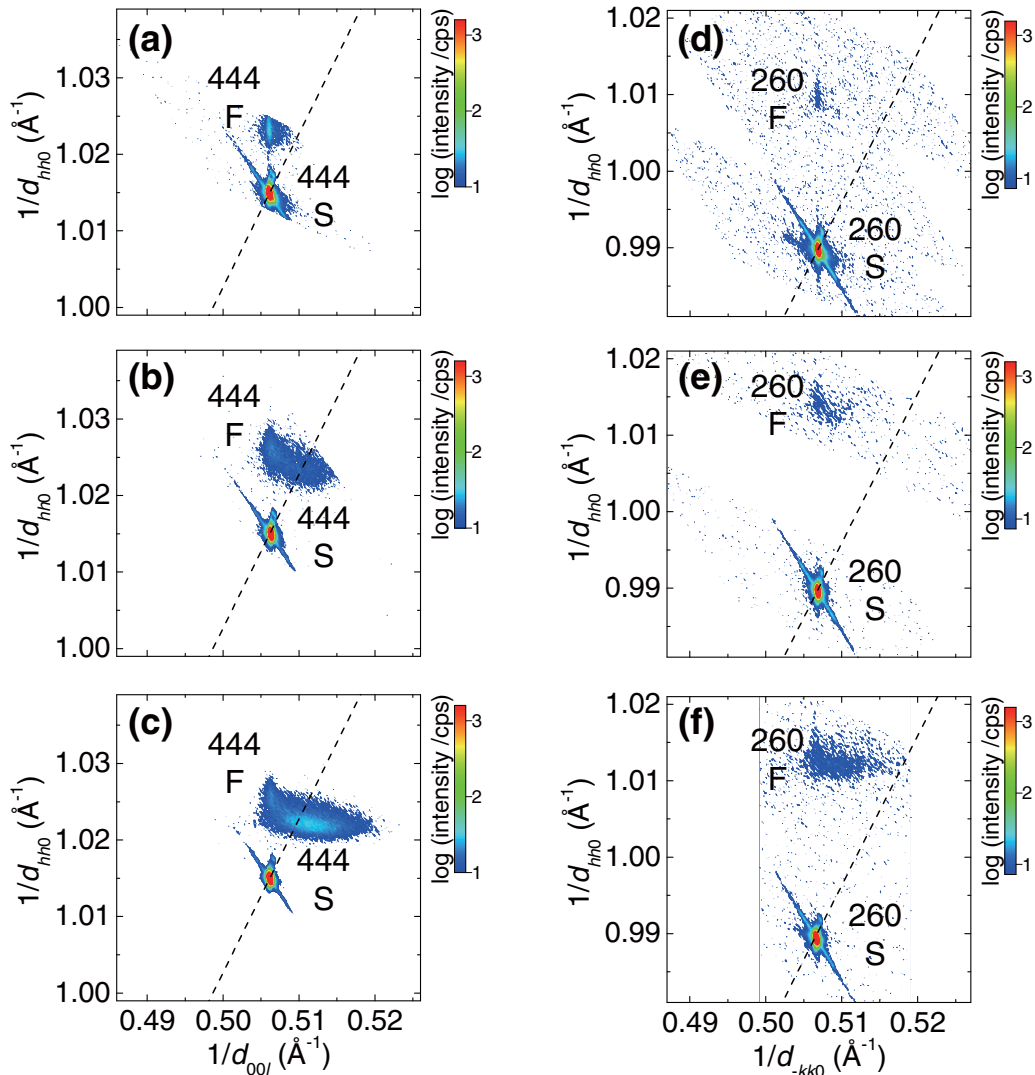


FIG. 3. Epitaxial structures of SCTO films on DSO substrates. Reciprocal space maps around (a)–(c) 444 and (d)–(f) 260 DSO reflections, of which in-plane  $d$  vectors are nearly orthogonal to each other. F and S denote reflections from films and substrates, respectively. Thicknesses of the films are (a), (d) 50 nm, (b), (e) 100 nm, and (c), (f) 170 nm.

order of  $10^{-1} \Omega \text{ cm}$  at room temperature and monotonically rose with decreasing temperature. Such an insulating behavior is contradictory to the bulk metallic SCTO [14]; the data of the bulk sample ( $\delta = 0.4$ ) were plotted with a dashed line for comparison. In order to investigate the effect of epitaxial strain, the temperature dependence of resistivity for the films (50–55 nm) on the NGO (110) and LSAT (100) substrates was also measured. The room-temperature resistivity of the film on LSAT was on the order of  $10^{-3} \Omega \text{ cm}$ , two orders of magnitude smaller than that on DSO. In addition, metallic conductivity was verified, although a slight upturn was seen at low temperatures ( $T < 60 \text{ K}$ ). Similar behaviors were found for the film on NGO, but strong metallicity remained down to 10 K.

The observed phenomena were also induced by varying film thickness. In general, the degree of epitaxial strain can be reduced as the films become thicker and begin to partially relax. We also grew films with thicknesses of 100 and 170 nm on DSO substrates, and measured their temperature dependence of resistivity. The room-temperature resistivity

systematically dropped with an increase in film thickness and became comparable to that on the LSAT substrate at 170 nm. These results also suggest that the observed MIT arises from epitaxial strain. It is worth mentioning that the low-temperature upturn in resistivity is seen only for samples in the vicinity of MIT, which is reminiscent of weak localization [16,23].

An epitaxial relationship was verified by using a four-circle XRD. Figures 3(a)–3(f) show reciprocal space maps (RSMs) of SCTO films on DSO substrates with various film thicknesses (50, 100, and 170 nm). Two reflections at around 444 and 260 were detected in order to measure strain along different crystallographic axes, i.e.,  $[\bar{1}10]$  and  $[001]$ . For the thinnest film, both of the in-plane lattice constants were identical to those of the substrate, indicating a coherent heterojunction. In contrast, the film reflections for the thicker ones (100 and 170 nm) expanded toward the origin axes (dashed lines), indicating that these films were partially relaxed. For 100-nm-thick film (middle panels), the logarithmic intensity of the coherent component was larger than that of the relaxed one.

TABLE I. Lattice constants of CTO, SmTO, SCTO, DSO, NGO, and LSAT.

Materials	$a$ (Å)	$b$ (Å)	$c$ (Å)	$d_{\bar{1}10}$ (Å)	$d_{002}$ (Å)	$d_{pc}$ (Å)
CTO	5.388	5.447	7.654	3.831	3.827	3.829
SmTO	5.467	5.669	7.742	3.938	3.871	3.915
SCTO	5.403	5.556	7.696	3.884	3.849	3.872
DSO	5.440	5.717	7.903	3.946	3.952	3.946
NGO	5.431	5.499	7.710	3.864	3.855	3.861
LSAT	3.868					3.868

In contrast, the relaxed component was the majority for the thickest film (170 nm). The difference in the epitaxial structure as a function of film thickness notably reflected the difference in resistivity; tensile-strained SCTO was insulating and the nearly relaxed film (170 nm) was metallic.

For a quantitative comparison of epitaxial strain, let us consider the lattice constants of the related compounds (CTO, SmTO, SCTO, DSO, NGO, and LSAT) listed in Table I. Except for SCTO, all the lattice constants were referred from the literature [12,13,24–27]. Both SmTO and CTO are GdFeO<sub>3</sub>-type structures with lattice constants of  $a = 5.467$ ,  $b = 5.669$ ,  $c = 7.742$  Å and  $a = 5.388$ ,  $b = 5.447$ ,  $c = 7.654$  Å, respectively [12,13,20]. Given a GdFeO<sub>3</sub>-type SCTO structure, the lattice constants of  $a = 5.428$ ,  $b = 5.558$ ,  $c = 7.698$  Å could be deduced from those of the parent compounds, according to the Vegard's law [12,13]. The calculated lattice constants were much closer to those of NGO ( $a = 5.431$ ,  $b = 5.499$ ,  $c = 7.710$  Å).

Pseudocubic  $d$  values ( $d_{pc}$ ) of the above-mentioned materials were calculated by the equation  $d_{pc} = \sqrt[3]{\frac{abc}{4}}$ . We also calculated the in-plane lattice constants (orthorhombic notation) as  $d_{\bar{1}10} = \frac{\sqrt{a^2+b^2}}{2}$  and  $d_{002} = \frac{c}{2}$ . The  $d_{pc}$ ,  $d_{\bar{1}10}$ , and  $d_{002}$  values of the related compounds are also listed in Table I. The  $d_{pc}$  of SCTO (3.872 Å) was much closer to that of cubic LSAT ( $a = 3.868$  Å) and orthorhombic NGO ( $d_{pc} = 3.861$  Å). Using all the  $d$  values and the equations of  $\varepsilon_{pc} = \frac{d_{pc,sub} - d_{pc,SCTO}}{d_{pc,SCTO}}$ ,  $\varepsilon_{\bar{1}10} = \frac{d_{\bar{1}10,sub} - d_{\bar{1}10,SCTO}}{d_{\bar{1}10,SCTO}}$ , and  $\varepsilon_{001} = \frac{d_{002,sub} - d_{002,SCTO}}{d_{002,SCTO}}$ , where  $\varepsilon$  is the lattice mismatch and its subscript defines the types of the components, the lattice mismatches of the substrates (sub) to the SCTO films (SCTO) were calculated and listed in Table II. The obtained values are also referred to as the magnitude of strain in the case where films are coherently grown on substrates. First, the degree of epitaxial strain was simply discussed based on the pseudocubic lattice mismatch ( $\varepsilon_{pc}$ ). Given the pseudocubic crystal symmetry, a little epitaxial strain was applied to the metallic SCTO films on LSAT and

TABLE II. Lattice mismatches of DSO, NGO, and LSAT to the SCTO films.

	$\varepsilon_{\bar{1}10}$ (%)	$\varepsilon_{001}$ (%)	$\varepsilon_{pc}$ (%)
SCTO/DSO	1.59	2.66	1.91
SCTO/NGO	-0.51	0.16	-0.28
SCTO/LSAT	-0.42	0.49	-0.11

NGO substrates (absolute  $\varepsilon_{pc}$  was less than 0.3%). Meanwhile, strong tensile strain ( $\varepsilon_{pc} \sim 2.0\%$ ) that was applied to the films on DSO substrates was likely to occur at 50-nm thickness on DSO. Therefore, we concluded that a strain-induced MIT emerged in our samples.

In addition to  $\varepsilon_{pc}$ , an in-plane biaxial lattice mismatch ( $\varepsilon_{\bar{1}10}$  and  $\varepsilon_{001}$ ) was also crucial for the properties of metallic SCTO films [28,29]. As shown in Fig. 2, the difference in resistivity and metallicity between the films on NGO and LSAT was significant despite similar  $d_{pc}$  values. This result can be understood if the biaxial lattice mismatch is taken into account. The SCTO film on LSAT substrates (smallest absolute  $\varepsilon_{pc}$ ) exhibited a relatively large biaxial lattice mismatch along both  $[\bar{1}10]$  and  $[001]$  directions ( $\varepsilon_{\bar{1}10} = -0.42\%$  and  $\varepsilon_{001} = 0.49\%$ ). They may compensate each other, leading to apparently small  $\varepsilon_{pc}$ . For the SCTO and NGO pair, they better matched along the  $[001]$  direction despite a largely nonuniform lattice mismatch ( $\varepsilon_{\bar{1}10} = -0.51\%$  and  $\varepsilon_{001} = 0.16\%$ ) and relatively large  $\varepsilon_{pc}$  ( $-0.28\%$ ). A smaller  $\varepsilon_{001}$  and common GdFeO<sub>3</sub>-type structures would have led to the realization of a higher crystalline quality and metallicity comparable to that of bulk SCTO [14]. In fact, a smaller FWHM of 0.068° was found in an x-ray rocking curve of the 220 SCTO reflection (not shown).

Strain-induced changes in electronic structures across MIT were also investigated by comparing two HXPES spectra for  $\sim 50$ -nm-thick SCTO films on DSO and LSAT substrates. In order to prevent the film surface from oxidation and/or contamination, amorphous Al<sub>2</sub>O<sub>3</sub> capping layers ( $\sim 5$  nm) were deposited at room temperature. Figure 4(a) shows the Sm 3d core-level spectra of SCTO films on DSO and LSAT substrates. The spectra were in good agreement with the Sm 3d spectrum of Sm<sub>2</sub>O<sub>3</sub> [30]. In addition, no sign of Sm<sup>2+</sup> and Sm<sup>0</sup> was found (see the inset); the Sm<sup>2+</sup> and Sm<sup>0</sup> components are expected to appear at  $\sim 1070$  eV, lower than the Sm<sup>3+</sup> component by  $\sim 10$  eV [31,32]. These results indicate that the Sm ions are in trivalent states in the SCTO films on both substrates. We confirmed that the Ca ions were in divalent states by measuring the Ca 2p core level (not shown).

Figure 4(b) shows the valence band spectra of the SCTO films on the DSO and LSAT substrates. The spectral shape closely matched between the samples. Since the 4f multiplet final states for Sm<sup>3+</sup> are spread over from 5 to 14 eV [33], the valence bands are mainly composed by the O 2p and Sm 4f states. The spectral feature detected near  $E_F$  arises from Ti 3d states. The relatively smaller Ti 3d contribution to the valence band spectra is owing to the smaller photoionization cross section [34].

To investigate the Ti 3d states in detail, magnified spectra near  $E_F$  are shown in Fig. 4(c). The Ti 3d states consisted of two-peak structures for each sample. The deeper and shallower peaks were observed at 2 and 1 eV, respectively. A clear gap opening in the SCTO film on DSO was found, while the SCTO film on LSAT showed a finite intensity at  $E_F$ . By comparing the observed spectra with those of La<sub>1-x</sub>Sr<sub>x</sub>TiO<sub>3</sub> [35,36], the photoemission intensity between  $E_F$  and 0.5 eV was emphasized in the SCTO films. Since the spectra for La<sub>1-x</sub>Sr<sub>x</sub>TiO<sub>3</sub> [35,36] were measured with  $h\nu = 21.2$  eV, the observed spectra strongly reflected the surface-sensitive electronic states. In addition, the electron

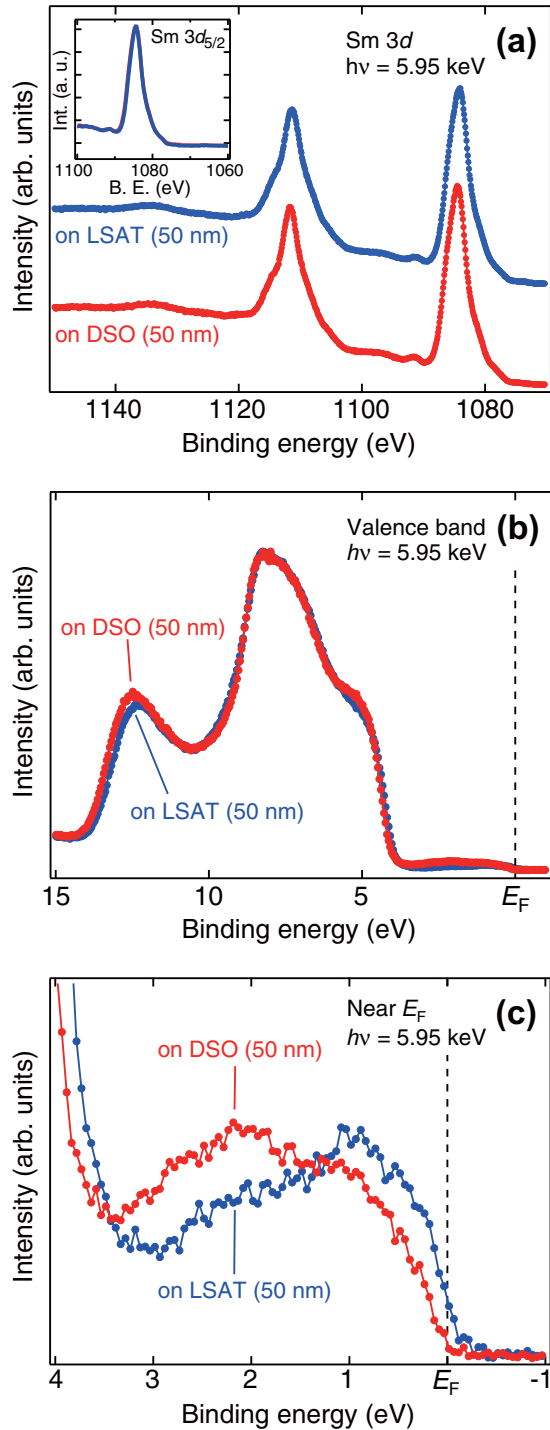


FIG. 4. Electronic structures of the SCTO films on the DSO (red) and LSAT (blue) substrates. (a) Sm  $3d$  core-level spectra. The inset shows the same photoemission spectra around the Sm  $3d_{5/2}$  core level expanded to the lower binding energy side. (b) Valence band spectra normalized by the highest intensity. (c) Magnified spectra near the Fermi level.

correlation effects at the surface were strong in many titanates and vanadates [37,38]. Therefore, the observed spectra for  $\text{La}_{1-x}\text{Sr}_x\text{TiO}_3$  showed a large discrepancy between the band calculation and experiment [35,36]. In contrast, it is known that the valence band spectra measured by HXPES reflect the

bulk-sensitive electronic states due to a large inelastic mean free path [39]. As a result of the bulk sensitivity in HXPES measurements, the photoemission intensity between  $E_F$  and 0.5 eV was emphasized in SCTO, reflecting the bandlike Ti  $3d$  states, that is, the coherent part. In contrast, the peaks located at 1 and 2 eV for the SCTO films showed a relatively high intensity. This result suggests that the electron correlation effects in the Ti  $3d$  states cannot be negligible and these two peaks would appear as an incoherent state (lower Hubbard band), while the appearance of two incoherent peaks is still unclear.

Let us consider the reason for the strong suppression of the states at  $E_F$  for the film on DSO. As seen in Fig. 4(c), the spectral weight of the Ti  $3d$  states near  $E_F$  is suppressed for the film on DSO in comparison to that on LSAT, which can be attributed to a Mott transition, as discussed below. The  $\text{GdFeO}_3$ -type structure (SCTO bulk) and the relationship between  $xyz$  and  $abc$  axes are shown in Fig. 5(a). For the (110)-oriented films, the  $y$  and  $z$  axes are designated as the orthogonal in-plane directions along  $[\bar{1}10]$  and  $[001]$ , respectively. Given a nearly cubic lattice in the films on NGO and LSAT as well as SCTO bulk,  $t_{2g}$  orbitals ( $d_{xy}$ ,  $d_{yz}$ , and  $d_{zx}$ ) at each Ti are threefold degenerate (orbital degeneracy  $N_d = 3$ ). In contrast, for the SCTO (50-nm) films on DSO, the threefold-degenerate orbitals split into two levels, nondegenerate lower  $d_{yz}$  and twofold-degenerate  $d_{zx}$  and  $d_{xy}$  orbitals, owing to the strong tensile strain ( $d_{001} \approx d_{\bar{1}10} > d_{110}$ ), hence  $N_d$  is reduced to 1 [see Fig. 5(b)].

$N_d$  is known to increase a critical  $U/W$  of MIT by a factor of  $\sqrt{N_d}$  [40,41], where  $U$  and  $W$  are the Coulomb repulsion and bandwidth, respectively. Therefore, the SCTO film on DSO should have a smaller critical  $U/W$  value than the SCTO bulk by a factor of  $1/\sqrt{3}$ . In Fig. 4 of Ref. [14], a phase boundary between metallic and insulating states for  $R_{1-x}\text{Ca}_x\text{TiO}_{3+y/2}$  has been shown to represent a straight line in a space of the inverse bandwidth ( $\tilde{W}^{-1}$ ) (a ratio of  $W^{-1}$  to that of  $\text{LaTiO}_3$ ) and hole concentration  $\delta (=x+y)$ . In the literature,  $\tilde{W}^{-1}$  for  $R = \text{Sm}$  is estimated to be  $\sim 1.14$  and a metallic state emerges above  $\delta \sim 0.24$ . Figure 5(c) shows a phase diagram with the horizontal and longitudinal axes inverted from the original ones ( $\delta$  vs  $\tilde{W}^{-1}$ ) so that the MIT boundary has a kink for the quarter-filled case ( $\delta = 0.5$ ), similar to the more popular  $U/W$  vs  $n$  diagram [5], where  $n$  is the  $3d$  band filling ( $n = 1 - \delta$ ). Here, SCTO bulk ( $N_d = 3$ ) is located at the upper part of the phase diagram. When the threefold-degenerate orbitals are lifted due to the strong tensile strain ( $N_d = 1$ ), the phase boundary is pushed downward by a factor of  $1/\sqrt{3}$  over  $\tilde{W}^{-1}$ . The tensile-strained SCTO is now located in the insulating region, which is consistent with the evolution of  $\rho$ - $T$  curves in Fig. 2. We suggest that a strain-induced modification of orbital degeneracy is responsible for the observed MIT in the present system.

In this regard, an application of compressive strain to SCTO will also provide a similar evolution of electronic properties. Namely,  $3d$  orbitals with  $N_d = 2$  in films under strong compressive strain are expected (twofold-degenerate lower  $d_{xy}$  and  $d_{zx}$  orbitals and a nondegenerate higher  $d_{yz}$  one), resulting in a slight push of the phase boundary toward smaller  $\tilde{W}^{-1}$ . Whether or not the orbital-degeneracy lifting scenario is likely in this system, it is an interesting experimental problem

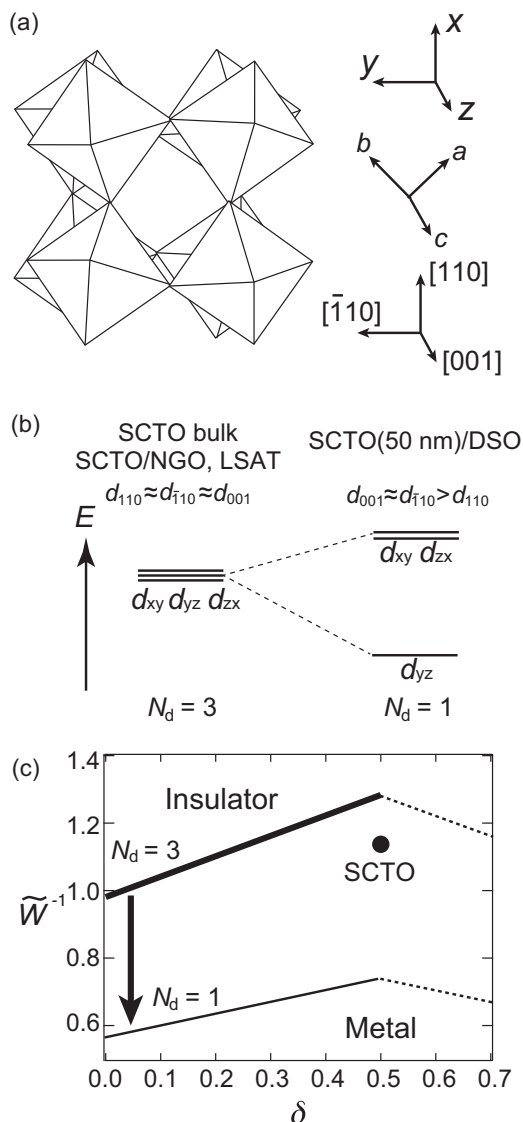


FIG. 5. (a) Schematic illustration of  $\text{GdFeO}_3$ -type perovskite structure.  $xyz$  and  $abc$  axes are defined in text. (b) Energy diagram of  $d_{xy}$ ,  $d_{yz}$ , and  $d_{zx}$  orbitals in SCTO bulk and films on DSO under strong tensile strain. (c) Schematic illustration of electronic phase diagrams for  $R_{1-x}\text{Ca}_x\text{TiO}_{3+y/2}$ . The phase boundary with the bold solid line is taken from Ref. [14]. The solid circle indicates SCTO. MIT in SCTO occurs when the orbital degeneracy ( $N_d$ ) is reduced from 3 to 1.

to be studied in the future. On the other hand, we admit that this scenario does not completely explain the MIT of SCTO films. The assumption that SCTO bulk is nearly cubic may be too simplified. In addition, the difference in  $\rho$ - $T$  curves between SCTO films on NGO and LSAT cannot be explained within the scenario. Considering the mismatch of atomic position, namely, oxygen octahedral rotation [42–44], the physical properties of the  $t_{2g}$  electron system would not solely depend on biaxial lattice mismatch, which is another interesting problem to be studied in future.

#### IV. CONCLUSION

In summary, we have demonstrated the strain-induced MIT of the distorted perovskite titanate of SCTO films. Using PLD, high-quality films were grown on isostructural perovskite with different lattice constants. The coherently grown film on DSO substrates showed insulating behavior, which was inconsistent with metallic bulk SCTO. The electronic structures of metallic and insulating SCTO films were investigated by HXPES. A suppression of DOS at  $E_F$  was found in the spectrum of the insulating film. These results indicate strain-induced MIT, rarely observed in  $t_{2g}$  electron systems of perovskite oxide with a weak Jahn-Teller effect on transition-metal ions. The growth of high-quality films of distorted perovskite oxides will be increasingly important to tackle the active control of exotic properties, such as multiferroics. In particular, the present results have demonstrated an ability to control the physical properties of perovskite titanates and would be usable for exploring functional ferroelectric and ferromagnetic materials such as  $\text{BaTiO}_3$  and  $R\text{TiO}_3$  ( $R = \text{Y}$  and/or late lanthanide ions).

#### ACKNOWLEDGMENTS

This work was partly supported by MEXT Elements Strategy Initiative to Form Core Research Center and a Grant-in-Aid for Scientific Research (No. 15H03881) from the Japan Society for the Promotion of Science Foundation. The synchrotron photoemission measurements were performed under the approval of the NIMS Synchrotron X-ray Station at SPring-8 (Proposal No. 2014B4701). The authors are grateful to the staff in HiSOR of Hiroshima University and JAEA/SPring-8 for the developing HXPES at BL15XU of SPring-8.

- [1] P. R. Willmott and J. R. Huber, Pulsed laser vaporization and deposition, *Rev. Mod. Phys.* **72**, 315 (2000).
- [2] M. Lorenz and M. S. R. Rao, 25 years of pulsed laser deposition, *J. Phys. D: Appl. Phys.* **47**, 030301 (2014).
- [3] Y. Konishi, Z. Fang, M. Izumi, T. Manako, M. Kasai, H. Kuwahara, M. Kawasaki, K. Terakura, and Y. Tokura, Orbital-state-mediated phase-control of manganites, *J. Phys. Soc. Jpn.* **68**, 3790 (1999).
- [4] K. Horiba, A. Maniwa, A. Chikamatsu, K. Yoshimatsu, H. Kumigashira, H. Wadati, A. Fujimori, S. Ueda, H. Yoshikawa, E. Ikenaga, J. J. Kim, K. Kobayashi, and M. Oshima, Pressure-induced change in the electronic structure of epitaxially strained  $\text{La}_{1-x}\text{Sr}_x\text{MnO}_3$  thin films, *Phys. Rev. B* **80**, 132406 (2009).
- [5] M. Imada, A. Fujimori, and Y. Tokura, Metal-insulator transitions, *Rev. Mod. Phys.* **70**, 1039 (1998).
- [6] Y. Tokura and N. Nagaosa, Orbital physics in transition-metal oxides, *Science* **288**, 462 (2000).
- [7] A. D. Rata, A. Herklotz, K. Nenkov, L. Schultz, and K. Dör, Strain-Induced Insulator State and Giant Gauge Factor of  $\text{La}_{0.7}\text{Sr}_{0.3}\text{CoO}_3$  Films, *Phys. Rev. Lett.* **100**, 076401 (2008).
- [8] Y. Okimoto, Y. Konishi, M. Izumi, T. Manako, M. Kawasaki, and Y. Tokura, Orbital-driven variation of electronic structures in tetragonal  $\text{La}_{1/2}\text{Sr}_{1/2}\text{MnO}_3$  as investigated by optical spectroscopy, *J. Phys. Soc. Jpn.* **71**, 613 (2002).
- [9] P.-H. Xiang, H. Yamada, A. Sawa, and H. Akoh, Strain-controlled electronic properties and magnetorelaxor behaviors

- in electron-doped  $\text{CaMnO}_3$  thin films, *Appl. Phys. Lett.* **94**, 062109 (2009).
- [10] P.-H. Xiang, S. Asanuma, H. Yamada, I. H. Inoue, H. Sato, H. Akoh, A. Sawa, K. Ueno, H. Yuan, H. Shimotani, M. Kawasaki, and Y. Iwasa, Strain-mediated phase control and electrolyte-gating of electron-doped manganites, *Adv. Mater.* **23**, 5822 (2011).
- [11] J. Fujioka, Y. Yamasaki, H. Nakao, R. Kumai, Y. Murakami, M. Nakamura, M. Kawasaki, and Y. Tokura, Spin-Orbital Superstructure in Strained Ferrimagnetic Perovskite Cobalt Oxide, *Phys. Rev. Lett.* **111**, 027206 (2013).
- [12] M. Mochizuki and M. Imada, Orbital physics in the perovskite Ti oxides, *New J. Phys.* **6**, 154 (2004).
- [13] H. D. Zhou and J. B. Goodenough, Localized or itinerant  $\text{TiO}_3$  electrons in  $\text{RTiO}_3$  perovskites, *J. Phys.: Condens. Matter.* **17**, 7395 (2005).
- [14] T. Katsufuji, Y. Taguchi, and Y. Tokura, Transport and magnetic properties of a Mott-Hubbard system whose bandwidth and band filling are both controllable:  $\text{R}_{1-x}\text{Ca}_x\text{TiO}_{3+y/2}$ , *Phys. Rev. B* **56**, 10145 (1997).
- [15] Y. Tokura, Y. Taguchi, Y. Okada, Y. Fujishima, T. Arima, K. Kumagai, and Y. Iye, Filling Dependence of Electronic Properties on the Verge of Metal-Mott-Insulator Transitions in  $\text{Sr}_{1-x}\text{La}_x\text{TiO}_3$ , *Phys. Rev. Lett.* **70**, 2126 (1993).
- [16] C. He, T. D. Sanders, M. T. Gray, F. J. Wong, V. V. Mehta, and Y. Suzuki, Metal-insulator transitions in epitaxial  $\text{LaVO}_3$  and  $\text{LaTiO}_3$  films, *Phys. Rev. B* **86**, 081401(R) (2012).
- [17] J. H. Ngai, T. C. Schwendemann, A. E. Walker, Y. Segal, F. J. Walker, E. I. Altman, and C. H. Ahn, Achieving A-site termination on  $\text{La}_{0.18}\text{Sr}_{0.82}\text{Al}_{0.59}\text{Ta}_{0.41}\text{O}_3$  substrates, *Adv. Mater.* **22**, 2945 (2010).
- [18] R. Dirsyte, J. Schwarzkopf, G. Wagner, R. Fornari, J. Lienemann, M. Busch, and H. Winter, Thermal-induced change in surface termination of  $\text{DyScO}_3$  (110), *Surf. Sci.* **604**, L55 (2010).
- [19] T. Ohnishi, K. Takahashi, M. Nakamura, M. Kawasaki, M. Yoshimoto, and H. Koinuma, A-site layer terminated perovskite substrate:  $\text{NdGaO}_3$ , *Appl. Phys. Lett.* **74**, 2531 (1999).
- [20] S. Ueda, Y. Katsuya, M. Tanaka, H. Yoshikawa, Y. Yamashita, S. Ishimaru, Y. Matsushita, and K. Kobayashi, Present status of the NIMS contract beamline BL15XU of SPring-8, in *SRI 2009, 10th International Conference on Radiation Instrumentation*, edited by R. Garrett, I. Gentle, K. Nugent, and S. Wilkins, AIP Conf. Proc. No. 1234 (AIP, Melville, NY, 2010), p. 403.
- [21] S. Ueda, Application of hard X-ray photoelectron spectroscopy to electronic structure measurements for various functional materials, *J. Electron Spectrosc. Relat. Phenom.* **190**, 235 (2013).
- [22] A. Ohtomo, D. A. Muller, J. L. Grazul, and H. Y. Hwang, Epitaxial growth and electronic structure of  $\text{LaTiO}_x$  films, *Appl. Phys. Lett.* **80**, 3922 (2002).
- [23] E. Abrahams, *50 Years of Anderson Localization* (World Scientific, Singapore, 2012).
- [24] R. H. Buttner and E. N. Maslen, Electron difference density and structural parameters in  $\text{CaTiO}_3$ , *Acta. Crystallogr., Sect. B* **48**, 644 (1992).
- [25] M. D. Biegalski, J. H. Haeni, S. Trolier-McKinstry, D. G. Schlom, C. D. Brandle, and A. J. Ven Graitis, Thermal expansion of the new perovskite substrates  $\text{DyScO}_3$  and  $\text{GdScO}_3$ , *J. Mater. Res.* **20**, 952 (2005).
- [26] B. Velickov, V. Kahlenberg, R. Bertram, and M. Bernhagen, Crystal chemistry of  $\text{GdScO}_3$ ,  $\text{DyScO}_3$ ,  $\text{SmScO}_3$ , and  $\text{NdScO}_3$ , *Z. Kristallogr.* **222**, 466 (2007).
- [27] M. Marezio, J. P. Remeika, and P. D. Dernier, Rare earth orthogallates, *Inorg. Chem.* **7**, 1337 (1968).
- [28] A. J. Millis, T. Darling, and A. Migliori, Quantifying strain dependence in “colossal” magnetoresistance manganites, *J. Appl. Phys.* **83**, 1588 (1998).
- [29] C. Adamo, X. Ke, H. Q. Wang, H. L. Xin, T. Heeg, M. E. Hawley, W. Zander, J. Schubert, P. Schiffer, D. A. Muller, L. Maritato, and D. G. Schlom, Effect of biaxial strain on the electrical magnetic properties of (001)  $\text{La}_{0.7}\text{Sr}_{0.3}\text{MnO}_3$  thin films, *Appl. Phys. Lett.* **95**, 112504 (2009).
- [30] C. Suzuki, J. Kawai, M. Takahashi, A.-M. Vlaicu, H. Adachi, and T. Mukoyama, The electronic structure of rare-earth oxides in the creation of the core hole, *Chem. Phys.* **253**, 27 (2000).
- [31] A. Yamasaki, A. Sekiyama, S. Imada, M. Tsunekawa, C. Dallera, L. Braicovich, T.-L. Lee, A. Ochiai, and S. Suga, Photoemission spectroscopy of  $\text{Sm}_4\text{As}_3$  using soft and hard x-rays, *J. Phys. Soc. Jpn.* **74**, 2538 (2005).
- [32] G. Dufour, R. C. Karnatak, J.-M. Mariot, and C. Bonnelle, Atomic and chemical effects in Sm and  $\text{Sm}_2\text{O}_3$  photoelectron spectra, *Chem. Phys. Lett.* **42**, 433 (1976).
- [33] G. K. Wertheim, The intermediate valence state in rare earth compounds, bulk and surface manifestations, *J. Electron Spectrosc. Relat. Phenom.* **15**, 5 (1979).
- [34] J. J. Yeh and I. Lindau, Atomic subshell photoionization cross sections and asymmetry parameters:  $1 \leq Z \leq 103$ , *At. Data Nucl. Data Tables* **32**, 1 (1985).
- [35] A. Fujimori, I. Hase, M. Nakamura, H. Namatame, Y. Fujishima, Y. Tokura, M. Abbate, F. M. F. de Groot, M. T. Czyzyk, J. C. Fuggle, O. Strebel, F. Lopez, M. Domke, and G. Kaindl, Doping-induced changes in the electronic structure of  $\text{La}_x\text{Sr}_{1-x}\text{TiO}_3$ : Limitation of the one-electron rigid-band model and the Hubbard model, *Phys. Rev. B* **46**, 9841 (1992).
- [36] T. Yoshida, A. Ino, T. Mizokawa, A. Fujimori, Y. Taguchi, T. Katsufuji, and Y. Tokura, Photoemission spectral weight transfer and mass renormalization in the Fermi-liquid system  $\text{La}_{1-x}\text{Sr}_x\text{TiO}_{3+y/2}$ , *Europhys. Lett.* **59**, 258 (2002).
- [37] A. Fujimori, I. Hase, H. Namatame, Y. Fujishima, Y. Tokura, H. Eisaki, S. Uchida, K. Takegahara, and F. M. F. de Groot, Evolution of the Spectral Function in Mott-Hubbard Systems with  $d^1$  Configuration, *Phys. Rev. Lett.* **69**, 1796 (1992).
- [38] A. Sekiyama, H. Fujiwara, S. Imada, S. Suga, H. Eisaki, S. I. Uchida, K. Takegahara, H. Harima, Y. Saitoh, I. A. Nekrasov, G. Keller, D. E. Kondakov, A. V. Kozhevnikov, Th. Pruschke, K. Held, D. Vollhardt, and V. I. Anisimov, Mutual Experimental and Theoretical Validation of Bulk Photoemission Spectra of  $\text{Sr}_{1-x}\text{Ca}_x\text{VO}_3$ , *Phys. Rev. Lett.* **93**, 156402 (2004).
- [39] K. Kobayashi, Hard x-ray photoemission spectroscopy, *Nucl. Instrum. Methods Phys. Res. A* **601**, 32 (2009).
- [40] O. Gunnarsson, E. Koch, and R. M. Martin, Mott transition in degenerate Hubbard models: Application to doped fullerenes, *Phys. Rev. B* **54**, R11026 (1996).
- [41] K. Yoshimatsu, T. Okabe, H. Kumigashira, S. Okamoto, S. Aizaki, A. Fujimori, and M. Oshima, Dimensional-Crossover-Driven Metal-Insulator Transition in  $\text{SrVO}_3$  Ultrathin Films, *Phys. Rev. Lett.* **104**, 147601 (2010).

- [42] D. Kan, R. Aso, H. Kurata, and Y. Shimakawa, Thickness-dependent structure-property relationships in strained (110) SrRuO<sub>3</sub> thin films, *Adv. Funct. Mater.* **23**, 1129 (2013).
- [43] Z. Liao, M. Huijben, Z. Zhong, N. Gauquelin, S. Macke, R. J. Green, S. Van Aert, J. Verbeeck, G. Van Tendeloo, K. Held, G. A. Sawatzky, G. Koster, and G. Rijnders, Controlled lateral anisotropy in correlated manganite heterostructures by interface-engineered oxygen octahedral coupling, *Nat. Mater.* **15**, 425 (2016).
- [44] D. Kan, R. Aso, R. Sato, M. Haruta, H. Kurata, and Y. Shimakawa, Tuning magnetic anisotropy by interfacial engineering the oxygen coordination environment in a transition metal oxide, *Nat. Mater.* **15**, 432 (2016).